Nuclear annihilation by antinucleons

Teck-Ghee Lee[1] and Cheuk-Yin Wong[2]
[1]*Department of Physics, Auburn University, Auburn, Alabama 36849, USA*
[2]*Physics Division, Oak Ridge National Laboratory, Oak Ridge, Tennessee 37831, USA*
(Received 18 September 2015; published 25 January 2016)

We examine the momentum dependence of $\bar{p}p$ and $\bar{n}p$ annihilation cross sections by considering the transmission through a nuclear potential and the $\bar{p}p$ Coulomb interaction. Compared to the $\bar{n}p$ annihilation cross section, the $\bar{p}p$ annihilation cross section is significantly enhanced by the Coulomb interaction for projectile momenta below $p_{\rm lab} < 500$ MeV/c, and the two annihilation cross sections approach the Pomeranchuk's equality limit [JETP Lett. **30**, 423 (1956)] at $p_{\rm lab} \sim 500$ MeV/c. Using these elementary cross sections as the basic input data, the extended Glauber model is employed to evaluate the annihilation cross sections for $\bar{n}$ and $\bar{p}$ interaction with nuclei and the results compare well with experimental data.

DOI: 10.1103/PhysRevC.93.014616

I. INTRODUCTION

In support of experiments of the FAIR (Facility for the Research with Antiprotons and Ions) at Darmstadt [1,2] and the AD (Antiproton Decelerator) at CERN [3] for antimatter investigations, it is of interest to continue our investigation on the annihilation between an antinucleon with nucleons or a nucleus that represent an important aspect of the interaction between antimatter and matter. A recent suggestion of using $\bar{n}A$ annihilation to study the n-$\bar{n}$ oscillations [4] provides an additional impetus to examine the annihilation between an $\bar{n}$ and a nucleus. In a recent work [5], we extended the Glauber model for nucleus-nucleus collisions [6–9] to study the antiproton-nucleus annihilation process. The extended Glauber model for the calculation of the $\bar{p}A$ annihilation cross section [5] consists of treating the nucleon-nucleus collision as a collection of binary collisions, with appropriate shadowing and the inclusion of initial-state and in-medium interactions. The basic ingredients are the elementary $\bar{p}p$ and $\bar{p}n$ annihilation cross sections, $\sigma_{\rm ann}^{\bar{p}p}$ and $\sigma_{\rm ann}^{\bar{p}n}$, together with initial-state Coulomb interactions and the change of the momentum of the antinucleon inside the nuclear medium. The model provides an analytical and yet intuitive way to analyze $\bar{p}$-nucleus annihilation processes. Qualitative features were reproduced to give a general map of the annihilation cross sections as a function of nuclear mass numbers and collision energies.

We would like to improve upon these earlier results on several important aspects. In our previous work, the basic $\bar{p}p$ annihilation cross section, $\sigma_{\rm ann}^{\bar{p}p}$, was parametrized semiempirically as $1/v$, the inverse of the relative velocity v, and utilized in our investigation of the stability and the properties of matter-antimatter molecules [11,12]. Such a simple dependence arises from the nuclear interaction between p and $\bar{p}$ in the s state and gives the main feature of the important momentum dependence of the annihilation cross section. Higher partial waves are also present and it is necessary to includes them properly. In addition to the nuclear interaction, p and $\bar{p}$ also interact through the attractive Coulomb interaction and $\sigma_{\rm ann}^{\bar{p}p}$ is expected to behave as $1/v^2$ in the lowest energy region [13,14]. It is of interest to examine the combined effects of the nuclear and Coulomb interactions to see how the $1/v$ behavior of the $\bar{p}p$ annihilation cross section is modified in the lowest energy region. A proper treatment of the Coulomb and nuclear interactions for $\sigma_{\rm ann}^{\bar{p}p}$ will also lead to a better determination of $\sigma_{\rm ann}^{\bar{n}p}$, which is expected to vary as $1/v$ at the lowest energies. Furthermore, in our earlier work in [5], $\sigma_{\rm ann}^{\bar{p}n}/\sigma_{\rm ann}^{\bar{p}p}$ was taken to be 4/5, based on the experimental ratio $(\sigma_{\rm ann}^{\bar{p}n})_D/(\sigma_{\rm ann}^{\bar{p}p})_D = 0.749 \pm 0.018$ for $\bar{p}$ at rest and 0.863 ± 0.018 for $\bar{p}$ in flight [15], and a model of nucleon-antinucleon annihilation by the annihilation of quark and antiquarks of the same flavor [5]. Because of the attractive Coulomb interaction is present in $p\bar{p}$ annihilation but absent in $\bar{p}n$ annihilation, $\sigma_{\rm ann}^{\bar{p}p}$ should be greater than $\sigma_{\rm ann}^{\bar{p}n}$ and the ratio $\sigma_{\rm ann}^{\bar{p}n}/\sigma_{\rm ann}^{\bar{p}p}$ should be energy dependent. Quark and antiquark can form a string and subsequently fragments, independent of the flavor contents of the quark and the antiquark. Thus, the approximate fixed ratio of $\sigma_{\rm ann}^{\bar{p}n}/\sigma_{\rm ann}^{\bar{p}p}$ of Ref. [5] should be amended and its energy dependencies must be properly taken into account.

On the theoretical side, there is the pioneering prediction of Pomeranchuk [16] on the equality of the annihilation cross section for $\bar{p}p$ and $\bar{p}n$ at high energies. One can envisage a q-$\bar{q}$ pairing model of nucleon-antinucleon annihilation in which the annihilation between a nucleon and an antinucleon takes place by pairing the valence quark of any flavor from the nucleon with any valence antiquark of any flavor from the antinucleon, with each q-$\bar{q}$ pair forming a string that subsequently fragments to many $\bar{q}q$ pairs (mesons), as in the string fragmentation in pp collisions [9,10]. At high energies when the long-range Coulomb effects become unimportant, such a q-$\bar{q}$ pairing model will predict the equality of $\sigma_{\rm ann}^{\bar{p}n} = \sigma_{\rm ann}^{\bar{p}p}$ because there are the same numbers of nine ways to combine the q and $\bar{q}$ pairs to form strings in $\bar{p}n$ and $\bar{p}p$ annihilations. An equality of $\sigma_{\rm ann}^{\bar{p}n} = \sigma_{\rm ann}^{\bar{p}p}$ at high energies will favor the q-$\bar{q}$ pairing model and is consistent with Pomeranchuk's prediction. It will exclude another annihilation model, as for example, the annihilation only by quarks of the same flavor [5].

To test Pomeranchuk's prediction and the annihilation models, we re-examine the basic cross sections of $\sigma_{\rm ann}^{\bar{p}n}$ and $\sigma_{\rm ann}^{\bar{p}p}$ to understand their similarities as well as their different energy dependencies. There are no experimental data of $\sigma_{\rm ann}^{\bar{p}n}$

for the collision of a $\bar{p}$ projectile with an isolated neutron target in free space. There are however experimental $\sigma_{\rm ann}^{\bar{n}p}$ annihilation cross section data using a $\bar{n}$ beam source (from the $\bar{p}p \to \bar{n}n$ reaction) colliding on a liquid hydrogen target [17,18], which are better suited for nucleon-antinucleon annihilation studies than those of [15] using the $\bar{p}$-(^{2}H) annihilations. As $\sigma_{\rm ann}^{\bar{n}p} = \sigma_{\rm ann}^{\bar{p}n}$, we shall therefore treat them equivalently and consider the problem of the annihilation of $\bar{p}$ on n to be equivalent to the problem of $\bar{n}$ on the target proton p.

To study the Coulomb and nuclear interactions of an antinucleon on the proton target, we shall assume for simplicity a square well potential of a fixed depth for which analytical results can be readily obtained [19]. The theoretical results and the comparison with experimental data allows one to draw a conclusion on Pomeranchuk's prediction and the annihilation models. Upon the determination of the improved basic $\sigma_{\rm ann}^{\bar{p}p}$ and $\sigma_{\rm ann}^{\bar{n}p}$ annihilation cross sections, they can then be used as the building blocks to evaluate the annihilation cross sections for antinucleons on a nucleus.

It is worth pointing out that over the years, a large set of experimental data in the annihilation of nucleons and nuclei by $\bar{p}$ and $\bar{n}$ had been accumulated [17,18,20–36] and analyzed theoretically [5,36–53]. Klempt, Batty, and Richard reviewed various phenomenological analyses of microscopic quark dynamics and symmetry considerations in nucleon-antinucleon annihilations. The roles of initial- and final-state interactions are also examined [36]. A theoretical optical potential based on the Glauber model [6,7] has been developed by Kuzichev, Lepikhin, and Smirnitsky to investigate the antiproton annihilation cross sections of various nuclei at the momentum range of 0.70–2.50 GeV/c [38]. In this range of relatively high antiproton momenta, the Glauber model gives a good agreement with the experimental data, with the exception of the deviations at the momentum of 0.7 GeV/c for heavy nuclei. Batty, Friedman, and Gal have developed a unified optical potential approach for low-energy $\bar{p}$ interactions with proton and with various nuclei using a density-folded optical potential [42,43]. They found that even though the density-folding potential reproduces satisfactorily the $\bar{p}$ atomic level shifts and widths across the periodic table for $A > 10$ and the few annihilation cross sections measured on Ne, it does not work well for He and Li. Galoyan, Uzshinsky, and collaborators have previously investigated cross sections of various processes in $\bar{p}p$ collisions in many different mechanisms. They have used different parametrizations of the basic total and elastic $\bar{p}p$ cross sections in the Glauber model and have successfully implemented these calculations in the GEANT4 program for the simulation of the passage of particles through matter in high-energy nuclear detector studies [45–53]. In the low-momentum regime ($p_{\rm lab} < 1$ GeV/c), however, many questions remain open to provide additional motivation for the present study. For example, how does the electrostatic Coulomb interaction between the collision pair affects the annihilation cross section as function of target mass A and charge numbers Z, and the projectile momentum in the laboratory frame $p_{\rm lab}$? And at approximately what momentum the contributions of the Coulomb interaction begins to be less effective? This study attempts to address these questions.

The paper is organized as follows. In Sec. II, we study the basic $\bar{p}p$ and $\bar{p}n$ annihilation cross sections by considering the effects of particles transmission through a nuclear potential barrier, initial-state Coulomb interaction between the collision pair and relativistic two-body kinematics. As the results for the present survey will not be sensitive to the fine structure of the potential well, we shall assume a square well potential for which analytical results for the transmission coefficients are well known. The experimental $\bar{p}p$ and $\bar{n}p$ annihilation cross sections can be successfully described in terms of transmission coefficients of various partial waves and Coulomb Gamow factors. In Sec. III, the basic $\bar{p}p$ and $\bar{n}p$ cross sections obtained in the theoretical analysis is then included in the extended Glauber model to calculate $\bar{p}$-nucleus collisions. The expressions are given for the $\bar{p}$-nucleus annihilation cross sections in terms of basic $\bar{p}$-nucleon annihilation cross section, $\sigma_{\rm ann}^{\bar{p}\text{-nucleon}}$. In Sec. IV, we assess the theory by comparing its numerical results to experimental data at both high and low energies, Finally, we conclude the present study with some discussions in Sec. V.

II. THEORY OF $\bar{p}p$ AND $\bar{n}p$ ANNIHILATION CROSS SECTIONS

To analyze the $\bar{p}p$ and $\bar{n}p$ annihilation cross section at a center-of-mass energy $E_{\rm c.m.}$, we follow Blatt and Weisskopf [19] to decompose the incoming plane waves into partial waves and we use the ingoing-wave strong absorption model to assume that a partial wave transmitted passing through the nucleon surface R will lead to a reaction, which in our case is an annihilation. In the case of $\bar{p}p$ annihilation, there is in addition the initial-state Coulomb interactions which can be taken into account through the Coulomb Gamow factor $G_L(k)$ [54] (or the K-factor $K(\eta)$ in [55,56]). The $\bar{p}p$ and $\bar{p}n$ annihilation cross sections for a collision with a wave number $k = \sqrt{2\mu E_{\rm c.m.}}$ and a reduced mass μ are then given in terms of the transmission coefficients T_L and the Gamow factor G_L by

$$\sigma_{\rm ann}(k) = \frac{\pi}{k^2} \sum_{L=0}^{L_{\rm max}} (2L+1) T_L(k) G_L(k), \tag{1}$$

where $G_L(k)$ is 1 for $\bar{p}n$ annihilation.

To calculate the transmission coefficients, we consider the nucleon and the antinucleon to interact through a nuclear interaction, which for simplicity can be taken to be a square well $V(r) = -V_0\Theta(R-r)$. The transmission coefficient is then given by Eq. (5.5) on p. 360 of [19] as

$$T_L = \frac{4 s_L K R}{\Delta_L^2 + (s_L + KR)^2}, \tag{2}$$

where $K = \sqrt{k^2 + 2\mu V_0}$,

$$s_L = R\left[\frac{g_L(df_L/dr) - f_L(dg_L/dr)}{g_L^2 + f_L^2}\right]_{r=R}, \tag{3}$$

$$\Delta_L = R\left[\frac{g_L(df_L/dr) + f_L(dg_L/dr)}{g_L^2 + f_L^2}\right]_{r=R}, \tag{4}$$

$$f_L(r) = \left(\frac{\pi kr}{2}\right)^{1/2} J_{L+1/2}(kr), \tag{5}$$

$$g_L(r) = -\left(\frac{\pi kr}{2}\right)^{1/2} N_{L+1/2}(kr), \tag{6}$$

where $J_{L+1/2}(kr)$ and $N_{L+1/2}(kr)$ are Bessel and Neumann functions, respectively. The Gamow factor for $\bar{p}p$ annihilation under the Coulomb interaction $V_c(r) = \alpha/r$ is [56]

$$G_L(k) = \frac{(L^2+\xi^2)[(L-1)^2+\xi^2]\cdots(1+\xi^2)}{[L!]^2} \times \left(\frac{2\pi\xi}{\exp\{2\pi\xi\}-1}\right), \tag{7}$$

where $\xi = \alpha/v$ and α is the fine structure constant. Following Todorov [57] and Eqs. (21.13a)–(21.13c) of Crater *et al.* [58], in the center of mass coordinate system, it is shown that the relative velocity v for two equal-mass particles with rest mass m is related to their center of mass $\sqrt{s}$ and can be expressed as [55]

$$v = \frac{(s^2-4sm^2)^{1/2}}{s-2m^2} \tag{8}$$

and

$$s = (a+b)^2 = (a_0+b_0)^2 - (\boldsymbol{a}+\boldsymbol{b})^2, \tag{9}$$

where $a = (a_0, \boldsymbol{a})$ and $b = (b_0, \boldsymbol{b})$ are the four-momentum vectors of the two colliding particles with a and b represent the target and projectile, respectively.

III. THE $\bar{p}p$ AND $\bar{n}p$ ANNIHILATION CROSS SECTIONS

Expression (1) shows that for the antinucleon-nucleon annihilation cross section all necessary information is contained in the magnitudes $T_L(k)$ and $G_L(k)$; they define the cross section completely. To determine $T_L(k)$ and hence the cross section, we assume the nuclear contact radius $R = 0.97$ fm and the strong interaction potential $V_0 = 85$ MeV. Figure 1 displays the $\sigma^{\rm ann}_{\bar{p}p}$ cross section result obtained with Eq. (1) as a function of $\bar{p}$ incident momenta. Clearly shown in Fig. 1(a) is the theoretical result fits the experimental data impressively well over a broad energy range. The different contributions to the cross section from $L = 0$–3 partial waves as a function of energy is demonstrated in Fig. 1(b). Strong momentum dependence is observed for all the partial waves. The S wave is obviously dominated at momentum below 240 MeV/c. As $p_{\bar{p}\rm lab}$ increases from 240 to 750 MeV/c, the contribution from the P wave becomes important. As the incident energy increases further, i.e., above 750 MeV/c, the D wave begins to dominate, and so forth.

At this point, we are interested not only in the magnitude of the cross section given in Eq. (1), but also in its behavior for smaller values of $p_{\bar{p}\rm lab}$. To examine the cross section behavior at low-energy limit, we restrict ourselves to the case where the entrance channel wave number $k \ll K$ and the S wave is dominant. This simplifies the analysis and helps to elucidate the essential points. According to Eq. (1), the annihilation

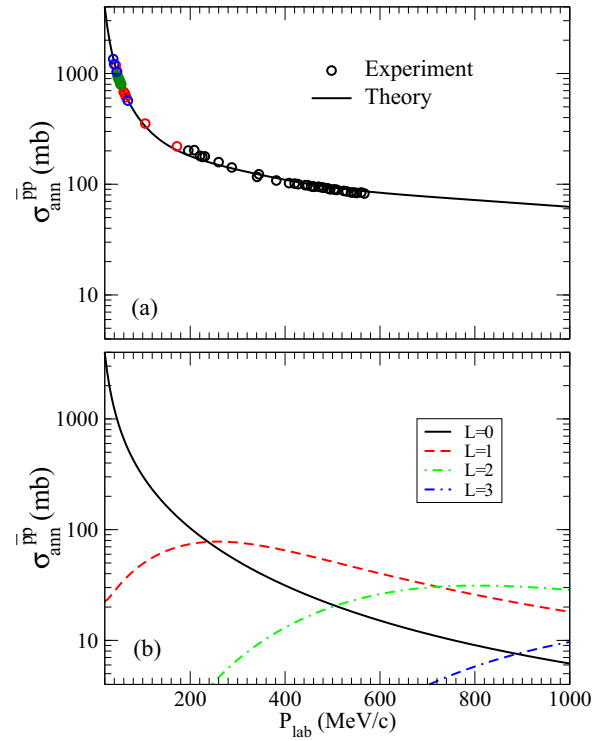

FIG. 1. (a) Antiproton-proton annihilation cross sections as a function of the antiproton momentum in the laboratory frame. The solid curve represents the $\bar{p}p$ annihilation cross section of Eq. (1). The experimental data points are from the compilation of [25], where the individual experimental sources can be found. (b) Contributions from different partial waves to the total annihilation cross sections.

cross section is reduced to

$$\sigma^{\rm ann}_{\bar{p}p} = \frac{\pi}{k^2} T_0(k) G_0(k) = \pi\left(\frac{4K}{k(K+k)^2}\right)\left(\frac{2\pi\xi}{\exp\{2\pi\xi\}-1}\right). \tag{10}$$

The first factor in the formula clearly displays the $1/v$ behavior for $k \ll K$ while the parameter $\xi \to \infty$ gives

$$\frac{2\pi\xi}{\exp\{2\pi\xi\}-1} \to \frac{2\pi\alpha}{v}. \tag{11}$$

In that event, the product of the two factors leads to $\sigma^{\rm ann}_{\bar{p}p} \propto 1/v^2$ behavior at low-energy limit. This $1/v^2$ law was first pointed out by Wigner [13] and now its discussions can be found in quantum mechanics textbooks [14,59].

Having demonstrated that Eq. (1) is capable of reasonably describing the experimental $\bar{p}p$ annihilation cross section for a wide momentum range, we next examine the $\bar{n}p$ annihilation cross section as a function of the antineutron momentum for which $G_L(k) = 1$. Fig. 2(a) shows a comparison between the theoretical and two sets of experimental data from Brookhaven National Laboratory (BNL) [18] and from the OBELIX Collaboration [17]. Relative to the $\bar{p}p$ measurements, the annihilation cross section data for $\bar{n}p$ still remains relatively sparse to date and contain significant degrees of uncertainties. The two sets of data fall within the error bars of each other. The OBELIX data at around $p_{\rm lab} \sim 200$–300 MeV/c

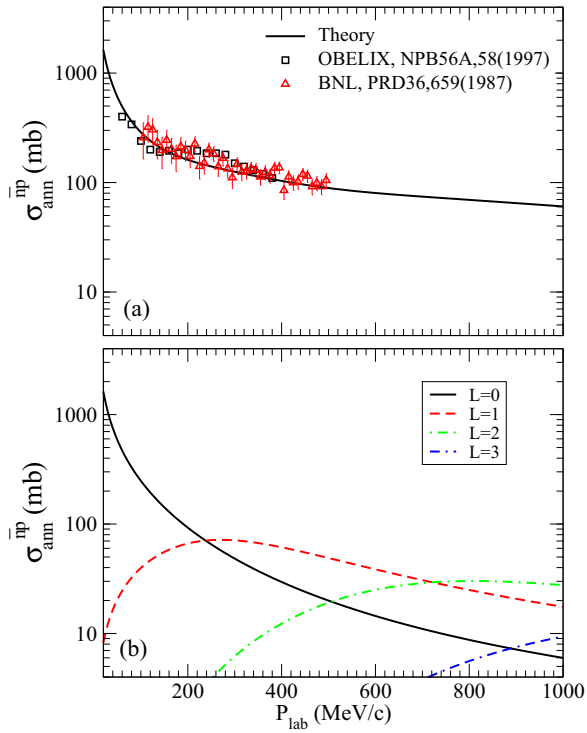

FIG. 2. (a) Antineutron-proton annihilation cross sections as a function of the antineutron momentum in the laboratory frame. Solid curve: $\bar{n}p$ annihilation cross section using Eq. (1) with the Gamow factor equal to 1. Solid triangle: experimental data from the OBELIX Collaboration [17] and open circle denotes experimental data from BNL [18]. (b) Contributions from different partial waves to the total annihilation cross sections.

appears to show an enhancement whereas the BNL data show greater fluctuation and appear to be qualitatively consistent with the theoretical predictions. Ultimately, we concur with Friedman's opinion [44] that the broad enhancement in the experimental finding for $\bar{n}p$ annihilation cross sections around 200–300 MeV/c [17] remains an open question.

Figure 3 indicates the importance of the Coulomb effect by comparing the $\bar{n}$ and $\bar{p}$ on proton annihilation as a function energy. The theoretical data are also plotted against the available experimental data. At high energy limit $p_{\rm lab} > 500$ MeV/c, both the $\bar{n}p$ and $\bar{p}p$ curves coincide. As $\sigma^{\bar{p}n}_{\rm ann} = \sigma^{\bar{n}p}_{\rm ann}$, the result in Fig. 3 validates the Pomeranchuk prediction [16] of $\sigma^{\bar{p}p}_{\rm ann} = \sigma^{\bar{p}n}_{\rm ann}$ for $p_{\rm lab} > 500$ MeV/c.

At the low-energy limit, it immediately becomes obvious that the slope for the $\bar{p}p$ interaction is much steeper compared to the $\bar{n}p$ one. Parametrizing the theoretical annihilation cross section in a power law form $\sigma_{\rm ann} \propto p^{x}_{\bar{p}\rm lab}$, the exponential value x can be simply obtained via $x = \partial ln(\sigma_{\rm ann})/\partial ln(p_{\bar{p}\rm lab})$. For the case of $\bar{p}p$, it is found that $x = -1.544$ in the momentum range between 30 and 50 MeV/c. Although it is not quite equal to $x = -2.0$ as expected to be at the low-energy limit [13,14], the behavior of the cross section is rightly approaching this limit as the projectile momentum further decreases. For the case of $\bar{n}p$, it is found that $x = -1.080$ in the momentum range between 30 and 95 MeV/c. Indeed, this exponential value is very close to the expected $x = -1.0$ value, a clear indication of the $1/v$

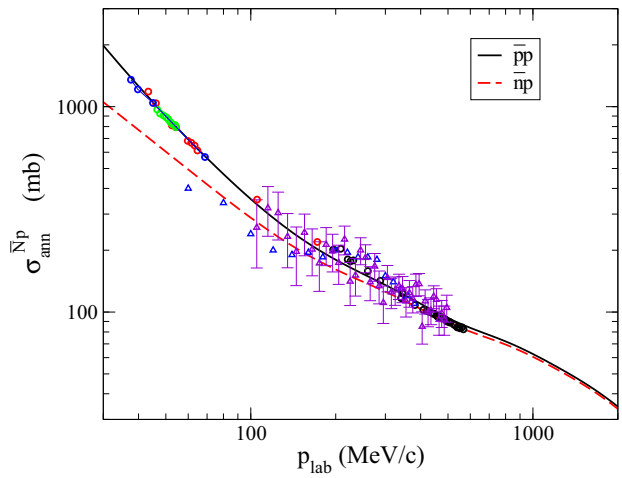

FIG. 3. Comparison of $\bar{p}p$ and $\bar{n}p$ annihilation cross sections as a function of the antiproton momentum in the laboratory frame.

behavior. The cross sections of these two cases have distinct power indices at low energies, depending on the charged or neutral character of the interaction pair.

IV. THE EXTENDED GLAUBER MODEL AND COMPARISON WITH EXPERIMENTAL $\sigma^{\bar{N}A}_{\rm ann}$ FOR $A > 1$ NUCLEI

The results in the last section pertain to the annihilation with $A = 1$ nucleus. To consider $\bar{p}$ or $\bar{n}$ annihilation with heavier $A > 1$ targets, we shall make use of our previously developed extended Glauber model. Because the derivations of the extended Glauber model are given in [5], here we review and emphasize only the essential formulas for describing $\bar{p}$ the experimental $\bar{p}$-nucleus annihilation cross sections for all energies and mass numbers. In the extended Glauber model, we first consider the incoming $\bar{p}$ travels along a linear trajectories as $\bar{p}$ approaches the nucleus and makes multiple collisions with the target nucleons along its way. The target and the projectile are represented by a density distribution function. For the target nucleus with small mass numbers $A < 40$, Gaussian density distribution function is considered. On the other hand, for the target nucleus with larger mass numbers, i.e., $A > 40$, uniform density distribution function with sharp-cut off is considered. The integral of the density distribution along the $\bar{p}$ trajectories gives the thickness functions which, in conjunction with the basic $\sigma^{\bar{p}p}_{\rm ann}$ and $\sigma^{\bar{p}n}_{\rm ann}$ annihilation cross sections, determines the probability for an $\bar{p}$-nucleon annihilation and consequently the high-energy $\bar{p}$-nucleus annihilation cross section

$$\begin{aligned}\sigma^{\bar{p}A}_{\rm ann}\left(\sigma^{\bar{p}-\rm nucleon}_{\rm ann}\right) &= \int d\boldsymbol{b}\Big\{1-\left[1-T_{\bar{p}p}(\boldsymbol{b})\sigma^{\bar{p}p}_{\rm ann}\right]^{Z}\\ &\quad\times\left[1-T_{\bar{p}n}(\boldsymbol{b})\sigma^{\bar{p}n}_{\rm ann}\right]^{N}\Big\}\\ &= \sum_{i=0}^{Z}\sum_{j=0}^{N}{}'\left(\frac{(-1)^{1+i+j}Z!N!}{(Z-i)!(N-j)!i!j!}\right)\\ &\quad\times\left(\sigma^{\bar{p}p}_{\rm ann}\right)^{i}\left(\sigma^{\bar{p}n}_{\rm ann}\right)^{j}\int d\boldsymbol{b}[T_{\bar{p}p}(\boldsymbol{b})]^{i}[T_{\bar{p}n}(\boldsymbol{b})]^{j},\end{aligned} \tag{12}$$

where $T_{\bar{p}p}$ and $T_{\bar{p}n}$ denote the thickness functions for protons and neutrons, respectively. The argument $\sigma_{\rm ann}^{\bar{p}-{\rm nucleon}}$ on the left-hand side stands for $\sigma_{\rm ann}^{\bar{p}p}$ and $\sigma_{\rm ann}^{\bar{p}n}$, and the summation $\sum_j'$ allows for all cases except when $i = j = 0$. The Z and N represent the number of protons and neutrons, respectively, in the nucleus.

To ensure Eq. (12) is also applicable for low-energy annihilation process, we extended the high-energy Glauber model by considering the Coulomb and nuclear interactions that are additional to those between the incoming antiproton and an annihilated target nucleon. The initial-state Coulomb correction resulted the modification of the projectile trajectory from linear to curved. The strong nuclear force, on the other hand, gives rise to the change of the antiproton momentum in the nucleus interior. The development of the extended Glauber model therefore resulted a compact $\bar{p}$-nucleus annihilation cross section

$$\Sigma_{\rm ann}^{\bar{p}A}(p_{\bar{p}\rm lab}) = \left\{1 - \frac{V_c(R_c)}{E}\right\}\sigma_{\rm ann}^{\bar{p}A}\left(\sigma_{\rm ann}^{p\bar{p}}(p''_{\bar{p}\rm lab})\right), \quad (13)$$

where

$$p''_{\bar{p}\rm lab} = p_{\bar{p}\rm lab}\sqrt{1 - \frac{\langle V_c(r)\rangle + \langle V_n(r)\rangle}{E}} \quad (14)$$

represents the change of the $\bar{p}$ momentum inside the nucleus due the average interior Coulomb $\langle V_c(r)\rangle$ and nuclear $\langle V_n(r)\rangle$ interactions. The $\{1 - V_c(R_c)/E\}$ factor on the other hand takes into account of the initial-state Coulomb effect that creates the path-deviation between the interaction pair from a straight-line trajectory with $V_c(R_c)$ is the Coulomb potential energy for $\bar{p}$ to be at the nuclear contact radius R_c and E is the center of mass kinetic energy of $\bar{p}$-nucleus collisions. This analytical formula is simple. Ultimately, to evaluate the $\bar{p}A$ or $\bar{n}A$ annihilation cross sections, one only needs to know the fundamental $\bar{p}p$ and $\bar{n}p$ annihilation cross sections.

We consider first the $\bar{p}A$ annihilation cross sections. In Fig. 4, the black solid curve represents the $\sigma_{\rm ann}^{\bar{p}p}$ we discussed earlier. The rest of the curves are results obtained from the extended Glauber model with the basic $\sigma_{\rm ann}^{\bar{p}p}$ and $\sigma_{\rm ann}^{\bar{p}n}$ obtained in the last section as input. Because $\sigma_{\rm ann}^{\bar{p}p}$ and $\sigma_{\rm ann}^{\bar{p}n}$ are slightly different from those we reported earlier [5], we find it necessary to readjust slightly some of the fitting parameters in the extended Glauber model in order to reproduce the experimental results. We use the same functional forms and notations of the geometrical parameters as in [5]. For a light nucleus with $A < 40$, we consider a Gaussian thickness function with the geometrical parameter $\beta^2 = \beta_A^2 + \beta_B^2 + \beta_{\bar{p}p}^2$, where $\beta_A = r_0' A^{1/3}$, $\beta_B = 0.68$ fm, and $\beta_{\bar{p}p} = \sigma_{\rm ann}^{\bar{p}p}/2\pi$. For a heavy nucleus with $A > 40$, we consider a uniform density distribution with the sharp cut-off thickness function and the geometrical parameters $R_c = R_A + R_B + \sqrt{\sigma_{\rm ann}^{\bar{p}p}/2\pi}$, where $R_A = r_0 A^{1/3}$ and $R_B = 0.95$ fm. The new parameters r_0, r_0', and nuclear potential depth $\langle V_n\rangle$ are tabulated in Table I. Here, we also find a slightly smaller radius parameter $r_0 = 1.00$ fm that gives a better description of the experimental data. It is worthwhile to note that in the present work all the parameter values r_0 and r_0' remain close to those used in [5].

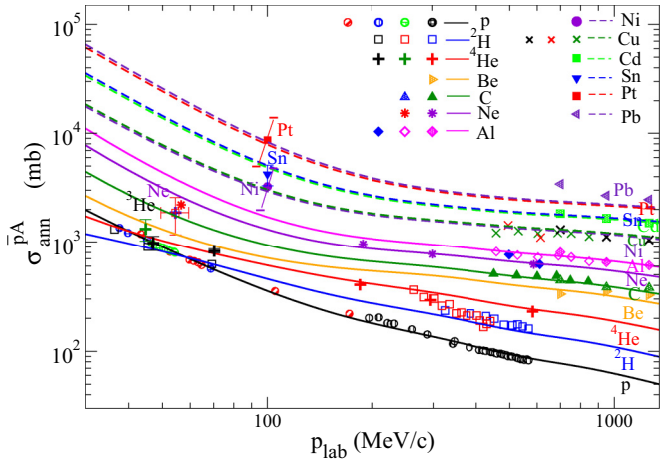

FIG. 4. $\bar{p}A$ annihilation cross sections as a function of the antiproton momentum in the laboratory frame. The experimental data are from Ref. [25]. The basic $\bar{p}p$ curve is calculated from Eq. (1) and the rest are from the extended Glauber model.

TABLE I. Fitting parameters.

Nuclei	Gaussian r_0'(fm)	Uniform r_0(fm)	$\langle V_n\rangle$(MeV)
^{2}H	1.20		−1.0
^{4}He	1.20		−4.0
Be	1.00		−20.0
C	1.00		−20.0
Ne	1.00		−35.0
Al	1.00		−35.0
Ni		1.00	−35.0
Cu		1.00	−35.0
Cd		1.00	−35.0
Sn		1.00	−35.0
Pt		1.00	−35.0
Pb		1.00	−35.0

The fits to the $\bar{p}A$ annihilation cross sections in the present manuscript in Fig. 4 are almost identical to our previous results in Fig. 1 of Ref. [5]. This indicates that the gross features of the $\bar{p}A$ annihilation cross sections is insensitive to the basic $\bar{p}p$ and $\bar{p}n$ cross sections, when the annihilation process is properly described. There is however only the minor difference that with $\bar{p}p$ and $\bar{p}n$ annihilation cross sections approaching each other at high energies, the new results describe better the $\bar{p}(^2H)$ annihilation cross section at around $p_{\rm lab} = 400$–600 MeV/c. The discrepancies of the $\bar{p}(^2H)$ annihilation cross section at around $p_{\rm lab} = 270$ MeV/c remains an unresolved theoretical and perhaps experimental problem that needs to be rechecked.

It is illuminating to clarify why the $\bar{p}$Pt annihilation cross section at $p_{\rm lab} = 100$ MeV/c is as large as 9000 mb, corresponding to a black disk of annihilation with a maximum impact parameter radius, $b_{\rm max}$, of about 17 fm, when the geometrical touching radius, $R_{\rm Pt} + R_{\bar{p}}$, is only about 8 fm. It should be pointed out that without the Coulomb initial-

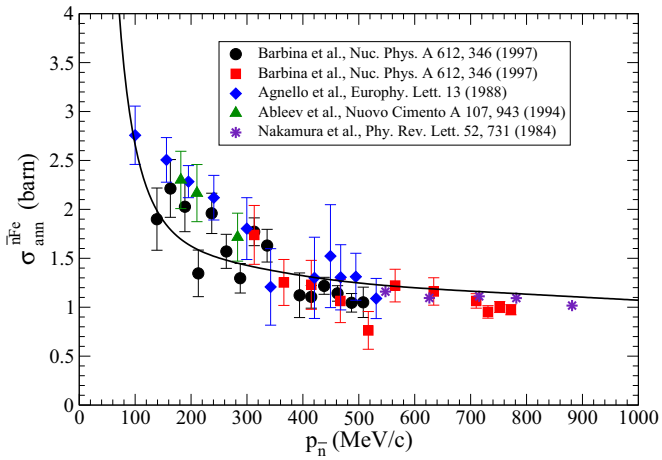

FIG. 5. $\bar{n}$Fe annihilation cross section as a function of the antineutron momentum in the laboratory frame. Comparing the result from Eq. (1) with several sets of experimental data.

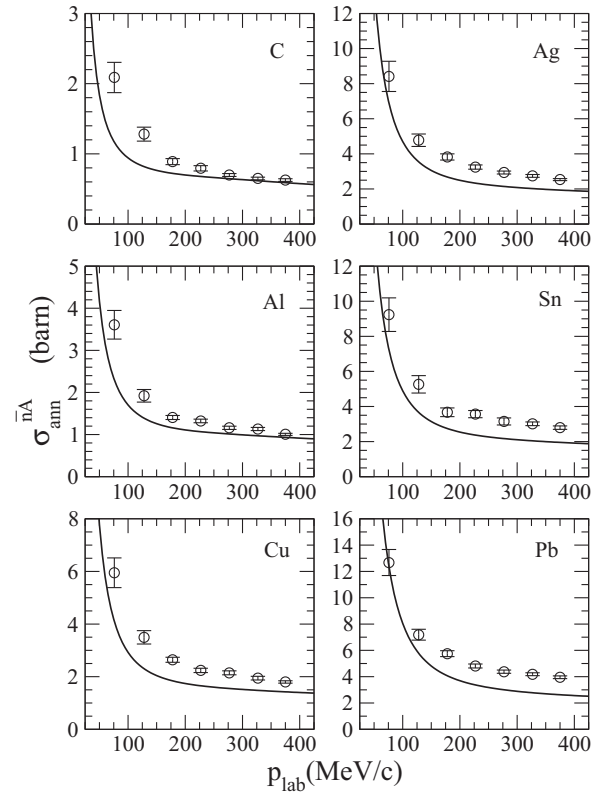

FIG. 6. $\bar{n}A$ annihilation cross section as a function of the antineutron momentum in the laboratory frame. Comparing the result from Eq. (1) with experimental data from [24].

state interaction for $\bar{p}$Pt annihilation, the extended Glauber model [the second factor $\sigma^{\bar{p}A}_{ann}$ in Eq. (13)] leads to a black-nucleus result for heavy nuclei, as the $\bar{p}$ particle makes multiple collisions and has many chances of annihilation with nucleons along its path in the nucleus. The black-nucleus cross section obtained in the extended Glauber model is approximately $\pi(b'_{max})^2 = \pi(R_{Pt} + R_{\bar{p}})^2 \sim \pi(8\ \text{fm})^2$, which is about 2000 mb. In the presence of the Coulomb initial-state interaction, the trajectory of a $\bar{p}$ at an impact parameter $b_{max} = 17$ fm will be pulled down to collide with the Pt nucleus at an impact parameter of $b'_{max} = 8$ fm, and the $\bar{p}$ is annihilated. The Coulomb enhancement factor $(1 - V_c(R_c)/E)$ in Eq. (13) corresponds to the ratio of b^2_{max}/b'^2_{max} and is about 4–5, which enhances the annihilation cross section from about 2000 mb to about 9000 mb, as indicated in Fig. 4.

We consider next the $\bar{n}A$ annihilation cross sections. Unfortunately, compared to the $\bar{p}A$ annihilation, experiments with antineutrons are to date scarce, in particular regarding their interaction with heavier nuclei. Nonetheless, there are a few have been reported in literature. Figure 5 shows the comparison of the result of extended Glauber model with the experimental cross section for $\bar{n}$Fe annihilation. The data indicate a strong dependence on the incoming $\bar{n}$ momentum, similar to that of the $\bar{n}p$ annihilation cross section discussed earlier. The theoretical results also appear to fit the experimental data reasonably well, suggesting the long-range Coulomb interaction is negligible despite the A value is large.

To better understand how well the present theory in describing the $\bar{n}A$ annihilation, it is necessary for us to examine the annihilation cross sections of $\bar{n}$ with other nuclei, namely C, Al, Cu, Ag, Sn, and Pb. Figure 6 shows the quality of agreement between the calculations and experimental data for projectile momentum $p_{\bar{n}} < 400$ MeV/c.

In Fig. 6, we observe, for the case of C and Al targets, the agreement between theoretical calculations and experimental data becomes poorer as one goes down in momentum. Contrasting this with the rest of the targets, the trend seems to go the opposite way. All said, even though the level of the overall agreement between the theoretical and experimental data within 20% is not that desirable, it is somewhat encouraging and not to mention the extended Glauber model has reasonably captured the main features of the annihilation cross sections for the energy range and mass numbers concerned. Unfortunately, at this point we cannot offer any reasonable explanation for the origin of the discrepancy between the theory and experiment. But we think that both theoretical and experimental investigations will be needed to clarify the situation.

V. DISCUSSION AND CONCLUSIONS

By considering the transmission through a nuclear potential and the $\bar{p}p$ Coulomb interaction, the nuclear annihilation cross sections can be properly evaluated in a simple analytical form. The present formulation is rigorous enough and therefore amends our earlier simple approach in which a semiempirical $1/v$ function has been employed in order to determine the basic $\sigma^{\bar{p}p}_{ann}$ and $\sigma^{\bar{p}n}_{ann}$ cross sections. The strong absorption model formulated here decomposes the incoming plane waves into a sum of partial waves of given orbital angular momentum L and assumes these partial waves transmit to the nucleon surface R leads to annihilation reaction. It is shown the cross sections for nuclear annihilation by $\bar{p}$ and $\bar{n}$ are simple functions of the momentum of the incident particles. Across the momenta range considered here, contrasting it to the $\sigma^{\bar{n}p}_{ann}$

annihilation cross section, the $\sigma_{\rm ann}^{\bar{p}p}$ annihilation cross section is significantly enhanced by the Coulomb interaction for the $p_{\rm lab}$ momenta of the incident particle below 500 MeV/c. As the $p_{\rm lab}$ increases, the two annihilation cross sections become almost identical, approaching the Pomeranchuk's equality limit at $p_{\rm lab} \sim 500$ MeV/c. In addition, the theoretical annihilation cross sections agree well with the experimental data. Concerning the broad enhancement in the experimental $\bar{n}p$ annihilation cross sections around 200–300 MeV/c, it is still a puzzle.

The equality of $\sigma_{\rm ann}^{\bar{p}n}$ and $\sigma_{\rm ann}^{\bar{p}p}$ at the limit of high energies predicted by Pomeranchuk can be perceived as a q-$\bar{q}$ pairing model in which the annihilation between a nucleon and an antinucleon takes place by pairing the valence quark of any flavor from the nucleon to any valence antiquark of any flavor from the antinucleon, with each q-$\bar{q}$ pair creating a string that subsequently fragments to many meson pairs [9,10]. Such model will explain the equality of $\sigma_{\rm ann}^{\bar{p}n}$ and $\sigma_{\rm ann}^{\bar{p}p}$ when the Coulomb effects become negligible at high energies. It overturns our naive quark model for annihilation—with annihilation takes place by pairing only the quark and antiquark of the same flavor.

Subsequently, with the help of these elementary cross sections, the extended Glauber model is used to evaluate the annihilation cross sections for the $\bar{p}$ and $\bar{n}$ interaction with other nuclear elements. For the case of $\bar{p}A$ interactions, we reproduced our previous results [5] and again these annihilation cross sections are found to be in good agreement with the measurements. For the case of $\bar{n}A$ interactions, predictions of the annihilation cross section are found to be in good agreement for Fe nuclei. However, for elements, C, Al, Cu, Ag, Sn, and Pb, agreement between the theory and experiments is found to be reasonable.

As it is now formulated, the behavior of the $\bar{p}A$ annihilation cross section at low energies varies as $1/E$ arising from the Coulomb enhancement factor, in addition to the energy dependencies of the basic $\bar{p}p$ and $\bar{p}n$ annihilation cross sections as described in Sec. III. Because these basic $\bar{p}p$ and $\bar{p}n$ annihilation cross sections increase substantially as the collision energy decreases, the granularity nature of the individual $\bar{p}p$ and $\bar{p}n$ collisions may not play a significant role in low-energy annihilations. A macroscopic description of the nucleus as a single potential without a granular structure may alternatively be a reasonable formulation. It will be of interest to re-examine the antinucleon-nucleus cross section at very low energies in a new light, by extending the potential approach as formulated in Sec. III for $\bar{p}p$ and $\bar{n}p$ annihilations to $\bar{p}A$ and $\bar{n}A$ annihilations in low-energy collisions. Future analysis along such lines will be of great interest.

ACKNOWLEDGMENTS

The authors would like to thank Dr. A. Galoyan for helpful discussions. The research was supported in part by the Division of Nuclear Physics, U.S. Department of Energy under Contract No. DE-AC05-00OR22725.

APPENDIX

Following [19], the expressions for the transmission coefficient $T_L(k)$ for $L = 1$, 2, and 3 partial waves

$$T_L(k) = \frac{4xXv_L}{X^2 + (2xX + x^2 v_L')v_L} \tag{A1}$$

with $x = kr$ and $X = KR$. The quantity $T_L(k)$ can be evaluated exactly with the functions v_L and v_L' given by

$$v_1 = \frac{x^2}{1+x^2}, \quad v_1' = \frac{1}{x^2} + \left(1 - \frac{1}{x^2}\right)^2, \tag{A2}$$

$$\begin{aligned} v_2 &= \frac{x^4}{9 + 3x^2 + x^4}, \\ v_2' &= \left(1 - \frac{6}{x^2}\right)^2 + \left(\frac{6}{x^3} - \frac{3}{x^2}\right)^2, \end{aligned} \tag{A3}$$

$$\begin{aligned} v_3 &= \frac{x^6}{225 + 45x^2 + 6x^4 + x^6}, \\ v_3' &= \left(1 - \frac{21}{x^2} + \frac{45}{x^4}\right) + \left(\frac{45}{x^3} - \frac{6}{x}\right)^2. \end{aligned} \tag{A4}$$

Similarly, following [56] with Eq. (76), the expressions for the Gamow factor

$$G_L(\xi) = \frac{(L^2+\xi^2)[(L-1)^2+\xi^2]\cdots(1+\xi^2)}{[L!]^2} \times \left(\frac{2\pi\xi}{\exp\{2\pi\xi\} - 1}\right) \tag{A5}$$

for $L = 1$, 2, and 3 partial waves can be evaluated using

$$G_0(\xi) = \frac{2\pi\xi}{\exp\{2\pi\xi\} - 1}, \tag{A6}$$

$$G_1(\xi) = \frac{1 + \frac{\alpha^2}{v^2}}{1^2} G_0(\xi), \tag{A7}$$

$$G_2(\xi) = \frac{\left[2^2 + \frac{\alpha^2}{v^2}\right]\left[1 + \frac{\alpha^2}{v^2}\right]}{(2!)^2} G_0(\xi), \tag{A8}$$

$$G_3(\xi) = \frac{\left[3^2 + \frac{\alpha^2}{v^2}\right]\left[2^2 + \frac{\alpha^2}{v^2}\right]\left[1 + \frac{\alpha^2}{v^2}\right]}{(3!)^2} G_0(\xi). \tag{A9}$$

[1] FAIR - Facility for Antiproton and Ion Research, Green Paper, October 2009.

[2] W. Erni *et al.* (PANDA Collaboration), Eur. Phys. J. A **49**, 25 (2013).

[3] S. Maury (for the AD Team), The Antiproton Decelerator (AD), CERN/PS 99-50 (HP) (1999).

[4] D. G. Phillips *et al.*, Neutron-Antineutron Oscillations: Theoretical Status and Experimental Prospects, arXiv:1410.1100.

[5] T. G. Lee and C. Y. Wong, Phys. Rev. C **89**, 054601 (2014).

[6] R. J. Glauber, in *Lectures in Theoretical Physics*, edited by W. E. Brittin and L. G. Dunham (Interscience, New York, 1959), Vol. 1, p. 315.

[7] R. Glauber and G. Matthiae, Nucl. Phys. B **21**, 135 (1970).
[8] C. Y. Wong, Phys. Rev. D **30**, 961 (1984).
[9] C. Y. Wong, *Introduction to High-Energy Heavy-Ion Collisions* (World Scientific Publisher, Singapore, 1994).
[10] See for example, references cited in C. Y. Wong, Phys. Rev. D **92**, 074007 (2015).
[11] C. Y. Wong and T. G. Lee, Ann. Phys. (NY) **326**, 2138 (2011).
[12] T. G. Lee, C. Y. Wong, and L. S. Wang, Chin. Phys. **17**, 2897 (2008).
[13] E. P. Wigner, Phys. Rev. **73**, 1002 (1948).
[14] L. D. Landau and E. M. Lifshitz, *Quantum Mechanics* (Pergamon, Oxford, 1958).
[15] T. E. Kalogeropoulos and G. S. Tzanakos, Phys. Rev. D **22**, 2585 (1980).
[16] I. Pomeranchuk, JETP Lett. **30**, 423 (1956).
[17] A. Bertin *et al.*, Nucl. Phys. B (Proc. Suppl. A) **56**, 227 (1997).
[18] T. Armstrong, C. Chu, J. Clement, C. Elinon, M. Furic, K. Hartman, A. Hicks, E. Hungerford, T. Kishimoto, J. Kruk, R. Lewis, D. Lowenstein, W. Lochstet, B. Mayes, R. Moss, G. S. Mutchler, L. Pinsky, G. A. Smith, L. Tang, W. vonWitsch, and Y. Xue, Phys. Rev. D **36**, 659 (1987).
[19] J. M. Blatt and V. F. Weisskopf, *Theoretical Nuclear Physics* (John Wiley and Sons, New York, 1952), p. 349.
[20] W. Brückner *et al.*, Z. Phys. A **335**, 217 (1990).
[21] A. Bertin *et al.* (OBELIX Collaboration), Phys. Lett. B **369**, 77 (1996).
[22] A. Benedettini *et al.*, Nucl. Phys. B (Proc. Suppl. A) **56**, 58 (1997).
[23] A. Zenoni *et al.* (OBELIX Collaboration), Phys. Lett. B **461**, 405 (1999).
[24] M. Astrua *et al.*, Nucl. Phys. A **697**, 209 (2002)
[25] A. Bianconi *et al.*, Phys. Lett. B **704**, 461 (2011).
[26] A. Bianconi *et al.*, Phys. Lett. B **481**, 194 (2000).
[27] A. Bianconi *et al.*, Phys. Lett. B **492**, 254 (2000).
[28] T R. Bizzarri *et al.*, Nuovo Cim. A **22**, 225 (1974).
[29] A. Zenoni *et al.* (OBELIX Collaboration), Phys. Lett. B **461**, 413 (1999).
[30] F. Balestra *et al.*, Phys. Lett. B **230**, 36 (1989).
[31] F. Balestra *et al.*, Phys. Lett. B **149**, 69 (1984).
[32] F. Balestra *et al.*, Phys. Lett. B **165**, 265 (1985).
[33] K. Nakamura *et al.*, Phys. Rev. Lett. **52**, 731 (1984).
[34] F. Balestra *et al.*, Nucl. Phys. A **452**, 573 (1986).
[35] V. Ashford *et al.*, Phys. Rev. C **31**, 663 (1985).
[36] E. Klempt, C. Batty, and J.-M. Richard, Phys. Rep. **413**, 197 (2005).
[37] J. Mahalanabis *et al.*, Nucl. Phys. A **485**, 546 (1988).
[38] V. F. Kuzichev, Yu. B. Lepikhin, and V. A. Smirnitsky, Nucl. Phys. A **576**, 581 (1994).
[39] J. Carbonell and K. Protasov, Hyperfine Interact. **76**, 327 (1993)
[40] J. Carbonell, K. Protasov, and A. Zenoni, Phys. Lett. B **397**, 345 (1997)
[41] A. Bianconi, G. Bonomi, E. LodiRizzini, L. Venturelli, and A. Zenoni, Phys. Rev. C **62**, 014611 (2000).
[42] A. Gal, E. Friedman, and C. J. Batty, Phys. Lett. B **491**, 219 (2000).
[43] C. J. Batty, E. Friedman, and A. Gal, Nucl. Phys. A **689**, 721 (2001).
[44] E. Friedman, Nucl. Phys. A **925**, 141 (2014).
[45] V. V. Uzhinsky and A. S. Galoyan, arXiv:hep-ph/0212369.
[46] A. S. Galoyan and A. Polanski, arXiv:hep-ph/0304196.
[47] A. Galoyan, J. Ritman, A. Sokolov, and V. Uzhinsky, arXiv:0809.3804.
[48] A. S. Galoyan and V. V. Uzhinsky, JETP Lett. **94**, 499 (2011) [Pisma Zh. Eksp. Teor. Fiz. **94**, 539 (2011)].
[49] V. Uzhinsky, J. Apostolakis A. Galoyan *et al.*, Phys. Lett. B **705**, 235 (2011).
[50] A. Galoyan and V. Uzhinsky, arXiv:1208.3614.
[51] A. Galoyan *et al.*, Hyperfine Interact. **215**, 69 (2013).
[52] A. Galoyan, PANDA Collaboration Report [B. P. Singh (Aligarh Muslim U.) *et al.*], Sept. 2, 2014, e-Print: arXiv:1409.0865 [hep-ex].
[53] A. Galoyan, PoS Baldin ISHEPP XXII 049 (2015).
[54] G. Gamow, Z. Phys. **51**, 204 (1928); see also L. I. Schiff, *Quantum Mechanics* (McGraw-Hill Company, New York, 1949), p. 117.
[55] L. Chatterjee and C. Y. Wong, Phys. Rev. C **51**, 2125 (1995).
[56] C. Y. Wong, Phys. Rev. D **60**, 114025 (1999). There is a typo error in Eq. (76) this reference. The denominator in Eq. (76), $[L!(2L+1)!!]^2$, should be $[L!]^2$ as in Eq. (A5).
[57] I. T. Todorov, Phys. Rev. D **3**, 2351 (1971).
[58] H. W. Crater, R. L. Becker, C. Y. Wong, and P. Van Alstine, Phy. Rev. D **46**, 5117 (1992).
[59] R. Newton, *Scattering Theory of Waves and Particles* (Springer-Verlag, New York/Heidelberg/Berlin, 1982).